Orientational ordering in solid C_{60} fullerene-cubane

Bart Verberck, Gerard A. Vliegenthart, and Gerhard Gompper

Citation: The Journal of Chemical Physics **130**, 154510 (2009); doi: 10.1063/1.3098550
View online: https://doi.org/10.1063/1.3098550
View Table of Contents: http://aip.scitation.org/toc/jcp/130/15
Published by the American Institute of Physics

Orientational ordering in solid C_{60} fullerene-cubane

Bart Verberck,[1,2,a)] Gerard A. Vliegenthart,[3] and Gerhard Gompper[2]
[1]*Departement Fysica, Universiteit Antwerpen, Groenenborgerlaan 171, B-2020 Antwerpen, Belgium*
[2]*Institut für Festkörperforschung, Forschungszentrum Jülich, D-52425 Jülich, Germany*
[3]*Institute for Advanced Simulation, Forschungszentrum Jülich, D-52425 Jülich, Germany*

(Received 11 December 2008; accepted 21 February 2009; published online 21 April 2009)

We study the structure and phase behavior of fullerene-cubane $C_{60}\cdot C_8H_8$ by Monte Carlo simulation. Using a simple potential model capturing the icosahedral and cubic symmetries of its molecular constituents, we reproduce the experimentally observed phase transition from a cubic to an orthorhombic crystal lattice and the accompanying rotational freezing of the C_{60} molecules. We elaborate a scheme to identify the low-temperature orientations of individual molecules and to detect a pattern of orientational ordering similar to the arrangement of C_{60} molecules in solid C_{60}. Our configuration of orientations supports a doubled periodicity along one of the crystal axes.
 [DOI: 10.1063/1.3098550]

I. INTRODUCTION

The recent synthesis of fullerene-cubane, $C_{60}\cdot C_8H_8$, by Pekker *et al.*[1] has marked the beginning of experimental[1–5] and theoretical[5] research on a new class of fullerene-containing crystals. While C_{60} fullerite, the solid built from C_{60} fullerene molecules [Fig. 1(a)] only,[6] was successfully doped with alkali atoms soon after its macroscopic production,[7] it took one and a half decade to come up with a crystal combining fullerenes with other molecules. Cubane [C_8H_8, Fig. 1(b)], the partner molecule, has eight carbon atoms arranged on the corners of a cube to each of which a hydrogen atom is bound. Interestingly, both constituents of $C_{60}\cdot C_8H_8$ were known experimentally well before its synthesis: C_8H_8 was first engineered in 1964 (Ref. 8) and C_{60} was discovered in 1985.[9] Each of the two molecules has a remarkably high symmetry: icosahedral (I_h) and cubic (O_h) for C_{60} and C_8H_8, respectively. In fact, the very existence of fullerene-cubane in 1:1 stoichiometry and its stability has been attributed by Pekker *et al.*[1] to the perfect matching of the two molecular geometries: at room temperature, the almost spherical C_{60} molecules leave voids at the octahedral interstices of a face-centered cubic (fcc) lattice into which a cubane molecule, having concave faces, fits perfectly.[10]

The room temperature phase of fullerene-cubane is well understood:[1,2] a binary fcc cubic structure (space group $Fm\bar{3}m$ and lattice parameter of $a=14.74$ Å) of freely rotating C_{60} molecules and nonrotating C_8H_8 molecules. Below $T\approx 140$ K, the crystal structure is orthorhombic, the C_{60} molecules do not rotate, and the cubane molecules maintain their fixed orientations. The static character of the cubane molecules was demonstrated by means of ^{1}H nuclear magnetic resonance (NMR) measurements;[1] the NMR spectrum remains unchanged when varying the temperature and has the fine structure of a static multispin system. The transition from rotating to nonrotating C_{60} molecules has been deduced from x-ray scattering measurements:[1,2,5,11] freely rotating C_{60} molecules lead to the appearance of a diffuse halo at $Q=3.3$ Å^{-1}. The room temperature phase has been termed "rotor-stator phase" by Pekker *et al.*[1] and the role of the cubane molecules as "molecular bearings" for the rotating fullerene molecules.

The phase transition in $C_{60}\cdot C_8H_8$ is similar to the structural transition in solid C_{60}: at room temperature, the C_{60} molecules in C_{60} fullerite are arranged on a fcc lattice and rotate nearly freely (space group $Fm\bar{3}m$),[12–16] while below $T\approx 249$ K, the molecules adopt well-defined orientations.[17–22] The low-T phase of solid C_{60} has space group $Pa\bar{3}$ (simple cubic Bravais lattice) and can be described as an ordering of the C_{60} molecules on four sublattices. The unit cell contains molecules at (0,0,0), $(a/2,a/2,0)$, $(a/2,0,a/2)$, and $(0,a/2,a/2)$, where a is the cubic lattice constant [$a=14.04$ Å at 5 K (Ref. 21)]. Starting from the so-called standard orientation, depicted in Fig. 2(a), each of these four molecules is rotated by the same setting angle ϕ about a local (i.e., molecular) threefold symmetry axis. For a C_{60} molecule in the standard orientation, four of its ten threefold axes coincide with the $\langle 111\rangle$ directions. The molecules in the unit cell are rotated about their local [111], $[1\bar{1}\bar{1}]$, $[\bar{1}\bar{1}1]$, and $[\bar{1}1\bar{1}]$ directions, respectively. The setting angle has been fitted to x-ray[18–20] and neutron[21] data; the best fits are obtained for 26° and 22°, respectively.[23] The resulting unit cell is shown in Fig. 2(b) (for $\phi=22°$). This structure has been interpreted as an optimal ordering scheme where pentagons (the centers of which are electron-poor) face electron-rich bonds fusing hexagons.[21] Comparing the transition temperatures of C_{60} fullerite and C_{60} fullerene-cubane shows that in the latter, the concavely shaped C_8H_8 molecules can indeed be seen as bearings facilitating the rotation of the C_{60} molecules.

In this paper we present a Monte Carlo (MC) simulation study of fullerene-cubane. We are mainly interested in the low-temperature phase, which is not yet completely understood.[1,2,5] Indeed, while x-ray powder diffraction has lead to the determination of the crystal system and lattice

a)Electronic mail: bart.verberck@ua.ac.be.

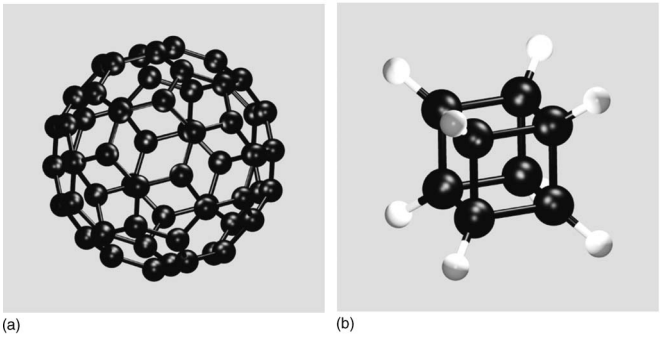

FIG. 1. A C_{60} molecule (a) and a C_8H_8 molecule (b), the two constituents of fullerene-cubane.

constants for $T<140$ K,[1,2] no space group has been proposed. Also, a periodicity doubling along one of the crystal axis has been suggested,[1] but the mechanism for it is unknown.

Apart from providing insight into the low-T crystal lattice, we want to investigate the rotational dynamics and statics of the C_{60} molecules. While it was concluded that at low temperature the C_{60} molecules do not rotate, precise orientations have not yet been inferred from experiments. Structural orientational properties have been studied in C_{60} fullerite, as discussed above, and in alkali fullerides. In AC_{60} alkali fullerides (A=K, Rb, or Cs),[7] a cubic-to-orthorhombic phase transition is accompanied by a transition from freely rotating to ordered C_{60} molecules as well: at T=350 K, C_{60} molecules polymerize into linear chains, oriented in specific ways within the crystal.[24–27] Such an orientationally ordered structure can be relevant for electronic properties, e.g., in polymerized K- and RbC_{60}, particular chain orientations are related to the absence/presence of an insulating state at low T.[25,28,29]

Because of the high symmetry and the almost spherical shape of a C_{60} molecule, energy differences arising from varying molecular orientations are small. For detecting subtle structural consequences of molecular reorientations, MC simulations provide an adequate tool. In Sec. II, we discuss the setup of our MC simulations. The essential ingredient of a MC simulation is a potential model for calculating molecular interaction energies; we address this issue in Sec. III. The evolution of the lattice structure with decreasing temperature and a detailed analysis of the low-T molecular orientations are discussed in Sec. IV, while Sec. V deals with translational aspects. Finally, a summarizing discussion and concluding remarks are presented in Sec. VI.

II. MC SIMULATIONS

The MC simulation technique allows the calculation of thermodynamic averages of physical quantities of many-body systems.[30,31] The central idea of MC simulations is to generate an ensemble—a set of configurations—of the system, in casu a $C_{60}\cdot C_8H_8$ crystal, obeying equilibrium statistics. We use the Metropolis acceptance rule[32] and perform MC simulations at constant number of molecules N, pressure p, and temperature T (NpT-ensemble) or at constant number of molecules N, volume V, and temperature T (NVT-ensemble). From the simulations in these two ensembles different properties are deduced.

We have taken $5\times5\times5$ orthorhombic face-centered unit cells with lattice constants A, B, and C, resulting in 4×5^3

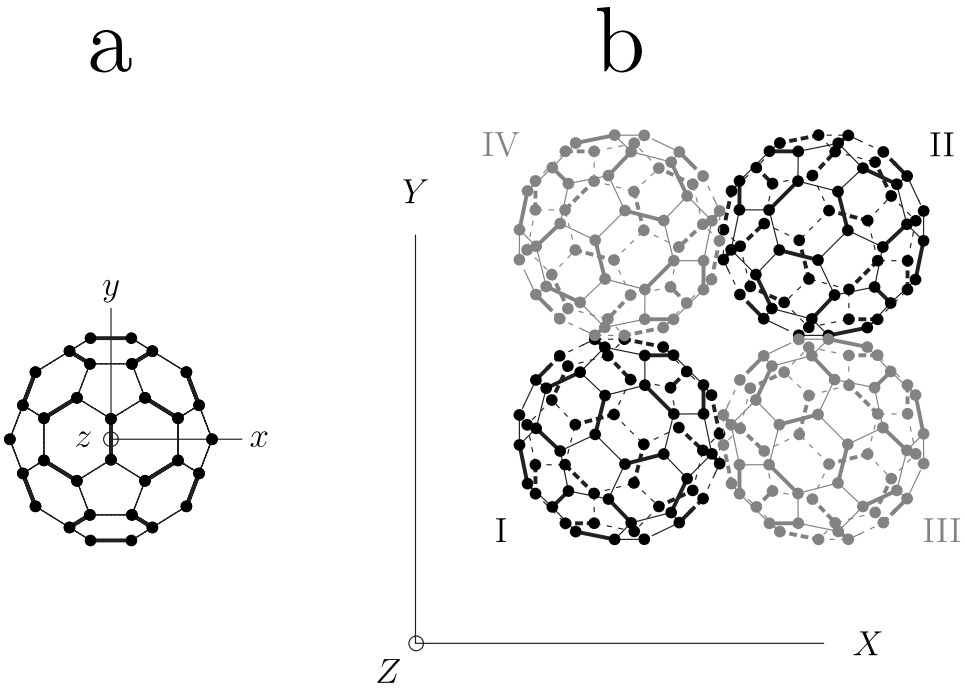

FIG. 2. (a) Projection onto the local (i.e., centered at the molecule's center of mass) (x,y)-plane of a C_{60} molecule in the standard orientation. Bonds fusing hexagons are shown bolder than bonds fusing hexagons and pentagons. (b) Unit cell of C_{60} fullerite, projected onto the crystallographic (X,Y)-plane. The molecules at (0, 0, 0) and $(a/2,a/2,0)$ are drawn in black, the molecules at $(a/2,0,a/2)$ and $(0,a/2,a/2)$ in gray. Dashed lines represent (parts of) bonds lying beneath the local (x,y)-plane. Labeling with Roman numerals has been introduced for later comparison.

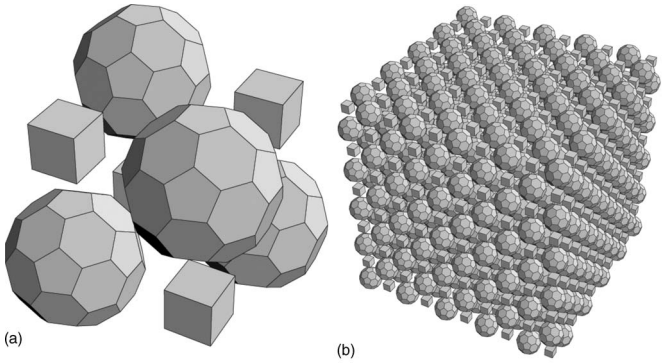

FIG. 3. (a) One fcc unit cell contains four C_{60} and four C_8H_8 molecules; (b) our simulation box is an array of $5\times5\times5$ such unit cells. Cubane and fullerene molecules are represented here by cubes and truncated icosahedra, respectively.

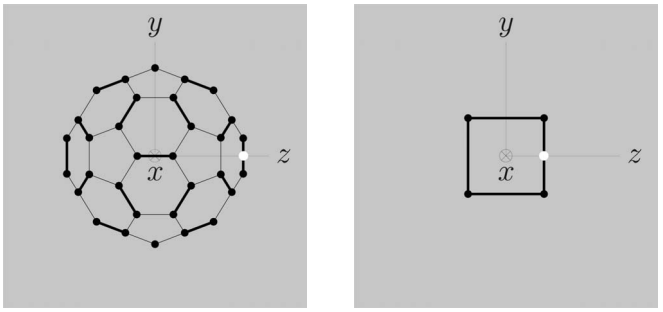

FIG. 4. (a) Projection onto the (y,z)-plane of a C_{60} molecule in the standard orientation [compare with Fig. 2(a)]. The coordinate axes coincide with twofold symmetry axes. The double bond with coordinates $(0,0,z_a=3.48\ \text{Å})$ is marked by a white dot. (b) Projection onto the (y,z)-plane of a C_8H_8 molecule—modeled as a cube—in the standard orientation. The cube's faces are parallel to the coordinate planes. The reference point with coordinates $(0,0,z_b)$ is indicated by a white dot.

$=500$ C_{60} and 500 C_8H_8 molecules and a simulation box of dimensions $L_X=5A$, $L_Y=5B$, and $L_Z=5C$ (Fig. 3). To describe the crystal, we introduce a Cartesian coordinate system (O,X,Y,Z), with lattice sites $\vec{X}(n_1,n_2,n_3)=n_1\vec{A}+n_2\vec{B}+n_3\vec{C}$, $\vec{A}=A\vec{e}_X$, $\vec{B}=B\vec{e}_Z$, and $\vec{C}=C\vec{e}_Z$. With each molecule, we associate a local Cartesian coordinate system (o,x,y,z) where the origin o coincides with the molecule's center of mass and the x-, y-, and z-axes are parallel to the X-, Y-, and Z-axes, respectively. We assume the molecules to be rigid, so each molecule has six degrees of freedom, three translational and three rotational. As a starting configuration, we assume the unit cells to be cubic $(A=B=C=14.74\ \text{Å})$ and put the centers of mass of the molecules at the exact fcc lattice positions and orient the molecules in their respective standard orientations (see Fig. 4).

In *NVT*-mode, a new configuration is obtained by randomly changing the position or the orientation of one molecule. Its potential energy is calculated and the Metropolis rule is applied to accept or reject the new configuration. We call this procedure a MC trial move. A sequence of MC trial moves is called a MC step; a single MC step consists of 10 000 MC trial moves: on average, 2500 translational C_{60}, 2500 translational C_8H_8, 2500 rotational C_{60}, and 2500 rotational C_8H_8 trial moves. The selection of the molecule and of the type of trial move (translational or rotational) is random.

In *NpT*-mode one has volume changes in addition to molecular displacements and rotations. In order to observe a transition from a cubic to an orthorhombic lattice, only one—randomly chosen—of the three box parameters is changed at a time, after which the new configuration is submitted to the Metropolis rule. Our *NpT*-mode MC steps include, apart from the 10 000 translational and rotational trial moves, ten such nonuniform volume trial changes.[33]

As usual in the simulations of bulk properties, periodic boundary conditions and the minimum-image convention have been implemented in our MC code. The maximal amplitudes of the translations, rotations, and volume changes have been chosen to yield acceptance rates of 50%. We have carried out simulations at atmospheric pressure for various temperatures in the range of $50\ \text{K}\leq T\leq 300\ \text{K}$. During the simulations, quantities such as total potential energy, density, pair distribution functions, lattice parameters, and translational and rotational mean-squared displacements were sampled in order to get insight into the phases of $C_{60}\cdot C_8H_8$.

III. MOLECULAR INTERACTIONS

A. Interaction potentials

The key ingredient of a MC simulation of a physical system is the calculation of its potential energy E. We assume that for a $C_{60}\cdot C_8H_8$ molecular crystal, the total potential energy is the sum of all intermolecular energies,

$$E=\frac{1}{2}\sum_{i_a}\sum_{j_a\neq i_a}E^{aa}(i_a,j_a)+\frac{1}{2}\sum_{i_b}\sum_{j_b\neq i_b}E^{bb}(i_b,j_b)+\sum_{i_a}\sum_{j_b}E^{ab}(i_a,j_b), \tag{3.1}$$

with indices i_a and j_a running over all fullerene molecules and i_b and j_b over all cubane molecules. Here and in the following, a stands for C_{60} and b for C_8H_8. We further make the approximation of pair interactions, i.e., every intermolecular energy is obtained as the sum of pair potentials. The $C_{60}-C_{60}$ interaction energy then reads as

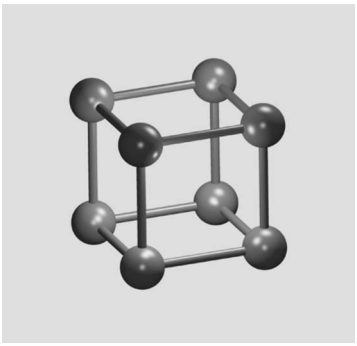

FIG. 5. We simplify a cubane molecule [Fig. 1(b)] to a cubic cluster of interaction centers, placed on the cubane molecule's C–H bonds.

$$E^{aa}(i_a,j_a)=\sum_{\lambda_a}\sum_{\lambda_a'} v^{aa}(|\vec{R}_{\lambda_a'}(j_a)-\vec{R}_{\lambda_a}(i_a)|), \tag{3.2}$$

where $\lambda_a=1,\ldots,60$ and $\lambda_a'=1,\ldots,60$ label the C atoms of the two interacting fullerene molecules i_a and j_a, respectively [see Fig. 1(a)]. In Eq. (3.2), the pair potential energy v^{aa} is evaluated at interatomic distances $|\vec{R}_{\lambda_a'}(j_a)-\vec{R}_{\lambda_a}(i_a)|$, with $\vec{R}_{\lambda_a}(i_a)$ the position of atom λ_a of molecule i_a and $\vec{R}_{\lambda_a'}(j_a)$ the position of atom λ_a' of molecule j_a. The atomic position $\vec{R}_{\lambda_a}(i_a)$ can be decomposed into the center-of-mass position $\vec{X}(i_a)$ and the local atomic position in the molecule $\vec{r}_{\lambda_a}$: $\vec{R}_{\lambda_a}(i_a)=\vec{X}(i_a)+\vec{r}_{\lambda_a}$. For $v^{aa}(r)$, we take the widely used truncated Lennard-Jones (LJ) potential,

$$v^{aa}(r)=\begin{cases}4\varepsilon^{aa}\left[\left(\dfrac{\sigma^{aa}}{r}\right)^{12}-\left(\dfrac{\sigma^{aa}}{r}\right)^{6}\right]+v_c^{aa} & \text{if } r<r_c^{aa}\\ 0 & \text{if } r\geq r_c^{aa},\end{cases} \tag{3.3}$$

with $v_c^{aa}=-4\varepsilon^{aa}[(\sigma^{aa}/r_c^{aa})^{12}-(\sigma^{aa}/r_c^{aa})^{6}]$ ensuring continuity at the cutoff distance r_c^{aa}, which we put at $r_c^{aa}=2.5\sigma^{aa}$. The 60 C atoms lie on a sphere with radius of $R=3.55$ Å. The molecular structure is actually not that of a regular truncated icosahedron but that of a nonregular truncated icosahedron: the edges of the pentagons are slightly longer than the edges fusing hexagons [single (s) and double (d) bonds, respectively]: $l_s=1.448$ Å and $l_d=1.404$ Å.[9]

Although choosing the 60 carbon atoms as interaction centers seems intuitively plausible, other, more refined, interaction models to describe C_{60}–C_{60} interactions in C_{60} fullerite have been developed over the years. One category of models assumes a distribution of electrostatic point charges on the C_{60} cage (maintaining overall charge neutrality), implying the addition of Coulomb interaction energies to the intermolecular potential energy.[34] Point charges need not only be located on the carbon atoms (vertices of the truncated icosahedron) but can also be located on the bonds of the C_{60} molecule (edges of the truncated icosahedron).[34] A further development is the use of three interaction centers (ICs) per double bond instead of one IC, reflecting the electronic density being smeared out along a double bond.[35] One of the better models agreeing well with x-ray diffuse scattering data on solid C_{60} (Ref. 36) has three ICs per double bond, one IC per single bond and every atom acting as an IC, with Born–Mayer–van der Waals pair potentials [$v(r)=C_1\exp(-C_2r)-B/r^6$, with C_1, C_2, and B potential constants depending on the types of ICs] and no point charges.[37] It is in this spirit that we model a cubane molecule as a cluster of eight ICs, one IC located on every C–H bond [see Figs. 1(b) and 5]. The location of the ICs—labeled $\lambda_b=1,\ldots,8$—on the C–H bonds is characterized by a dimensionless parameter $0\leq\xi\leq1$, with $\xi=0$ and 1 corresponding to the locations $\vec{r}_{C_{\lambda_b}}$ and $\vec{r}_{H_{\lambda_b}}$ of the C and the H atoms, respectively: $\vec{r}_{\lambda_b}=\vec{r}_{C_{\lambda_b}}+\xi(\vec{r}_{H_{\lambda_b}}-\vec{r}_{C_{\lambda_b}})$. (In cubane, carbons and hydrogens are located on spheres with radii $|\vec{r}_C|=1.353$ Å and $|\vec{r}_H|=2.449$ Å.[38]) In doing so, we avoid having two types of ICs (C and H), reducing the energy computation time, but we retain the cubic shape of the cubane molecule. We consider the parameter ξ as tunable, controlling the effective size of the cubane molecule. Since we also preserve the C_{60} molecule's icosahedral shape, we thus end up with a description of fullerene-cubane fully taking into account the symmetries of its constituting molecules. We argue that simplifying the cubane molecule to a cubic cluster of ICs is justified since the crystal structure of fullerene-cubane is interpreted as molecular recognition between the shapes of the C_{60} and the C_8H_8 molecules.[1] In our opinion, modeling $C_{60}\cdot C_8H_8$ as a system of icosahedral and cubic clusters of ICs is therefore a numerically feasible compromise between an all-atom description and a strongly simplified approach. The intercubane energies $E^{bb}(i_b,j_b)$ are then given by formulas completely analogous to Eqs. (3.2) and (3.3), replacing everywhere a by b. Fullerene-cubane energies are evaluated via the expression $E^{ab}(i_a,j_b)=\Sigma_{\lambda_a}\Sigma_{\lambda_b}v^{ab}(|\vec{R}_{\lambda_b}(j_b)-\vec{R}_{\lambda_a}(i_a)|)$ with $v^{ab}(r)$ as in Eq. (3.3) replacing aa by ab. The LJ potential parameters are obtained by applying the usual Lorentz–Berthelot mixing rules: $\sigma^{ab}=(\sigma^{aa}+\sigma^{bb})/2$ and $\varepsilon^{ab}=\sqrt{\varepsilon^{aa}\varepsilon^{bb}}$.

B. Potential constants

Our molecular interaction model contains five parameters: ε^{aa}, ε^{bb}, σ^{aa}, σ^{bb}, and ξ. Although five is a small number, trying out several combinations of these parameters is still time consuming. In view of the past work on modeling C_{60}–C_{60} interactions and the availability of established interaction potential models[36] as discussed above, we have chosen to fix ε^{aa} and σ^{aa} from the start. Out of the several LJ C–C potential parameter sets described in literature, we have arbitrarily chosen the values of Ref. 39—$\varepsilon^{aa}=28\text{K}\times k_B$ and $\sigma^{aa}=3.74$ Å. These parameters are close to other available values, e.g., $\varepsilon^{aa}=28\text{K}\times k_B$, $\sigma^{aa}=3.4$ Å (Ref. 40) and $\varepsilon^{aa}=33.25\text{K}\times k_B$, $\sigma^{aa}=3.47$ Å.[41]

As a first attempt to choose values for σ^{bb}, ε^{bb}, and ξ, we fitted the Born–Mayer–van der Waals potentials in Ref. 42 for C–C, C–H, and H–H interactions between aliphatic hydrocarbons to LJ potentials. Then, we performed a least-squares fit of the energy of two interacting cubane molecules—a cubane dimer $(C_8H_8)_2$—calculated with our cubic cluster model for several intermolecular distances averaged over various molecular orientations to the corresponding dimer energies obtained from the full aliphatic interaction potential taking C–C, C–H, and H–H interactions into account. This procedure yielded the values $\sigma^{bb}=2.07$ Å, $\varepsilon^{bb}=19.33K\times k_B$, and $\xi=0.4$.[5] Recently, *ab initio* energy calculations for several configurations of the cubane dimer have been performed by Nikolaev *et al.*[43] Two categories of energy calculations are presented, for varying intermolecular distance and varying molecular orientations. Fitting the cubic cluster LJ model to all the data sets in Ref. 43 simultaneously is impossible—a shortcoming of a general nature since any simple pair potential model never captures all the details of an intermolecular interaction. We do not need a highly accurate cubane-cubane potential since the $\frac{1}{2}\Sigma_{i_b}\Sigma_{j_b\neq i_b}E^{bb}(i_b,j_b)$ contribution to the total energy E is small anyway. Indeed, the typical distance between two nearest-neighbor C_8H_8 molecules in fullerene-cubane is

TABLE I. LJ potential parameters σ and ε, cutoff length r_c, and energy v_c for fullerene-fullerene (aa), cubane-cubane (bb), and fullerene-cubane (ab) interactions. Two parameter sets have been retained, differing in the choice of ξ and ε^{bb} (see text for details).

		Parameter set 1		Parameter set 2	
	aa	bb	ab	bb	ab
σ (Å)	3.74	2.05	$\frac{\sigma^{aa}+\sigma^{bb}}{2}=2.895$	2.05	2.895
$\varepsilon(\mathrm{K}\times k_B)$	28.0	5.0	$\sqrt{\varepsilon^{aa}\varepsilon^{bb}}=11.832$	10.0	16.733
$r_c=2.5\sigma$ (Å)	9.35	5.125	7.238	5.125	7.238
$v_c=-4\varepsilon\left[\left(\frac{\sigma}{r_c}\right)^{12}-\left(\frac{\sigma}{r_c}\right)^{6}\right](\mathrm{K}\times k_B)$	0.457	0.082	0.193	0.163	0.273

	Parameter set 1	Parameter set 2
ξ (dimensionless)	0.5	1.0

about 10 Å, well beyond the optimal 6.5 Å intermolecular distance.[43] We therefore considered the parameters σ^{bb}, ε^{bb}, and ξ as tunable, for our purposes, rather than to be taken from a fit to cubane-cubane interactions. *A priori* requirements for our potential constants are reproducing (i) a fcc phase with a lattice constant close to the experimental value $a=14.74$ Å at room temperature, (ii) a structural phase transition at about $T\approx 140$ K, and (iii) a transition from freely rotating to frozen fullerene molecules at about the same temperature as the structural phase transition.

To get started, we performed preliminary MC runs for a $4\times4\times4$ simulation box (containing $4\times4^3=256$ C_{60} and 256 C_8H_8 molecules) for several combinations of σ^{bb}, ε^{bb}, and ξ, with initial choices inspired by the values in Ref. 5 quoted above. We retained the two parameter sets quoted in Table I. Other sets we tried either resulted in too large room temperature lattice constants or in only slight differences from those obtained by one of the two selected parameter sets. Loosely speaking, parameter set 1 has smaller cubes and a shallower potential well than parameter set 2.

IV. *NpT*-ENSEMBLE SIMULATIONS

First, a sequence of equilibration *NpT*-mode MC steps has been generated for it is crucial to obtain thermodynamic equilibrium before starting to sample quantities and calculate their averages. During the equilibration, the total energy E is monitored; when it starts to fluctuate around a constant value, we assume that equilibrium has been reached. For each of the temperatures considered, the average energy E displays no drift. The quantities sampled in the *NpT*-mode are the lattice constants and orientational mean-squared displacements (OMSDs). The former determines the crystal system—cubic ($A=B=C$), tetragonal ($A=B\neq C$), or orthorhombic ($A\neq B\neq C$)—the latter quantifies molecular rotations (free rotations, quasifree rotations, or no rotations).

A. Energy and lattice constants

At any moment during the simulation, the box parameters L_X, L_Y, and L_Z are known; the lattice parameters are then simply obtained as $A=\langle L_X\rangle/5$, $B=\langle L_Y\rangle/5$, $C=\langle L_Z\rangle/5$.

In Figs. 6(a) and 6(b) we show the average energy and lattice constants for our two potential parameter sets. For parameter set 1, Fig. 6(a), we observe a cubic phase at room temperature and a transition to a tetragonal phase at about $T=110$ K. Below 90 K, it turns out to be difficult to determine the thermodynamically stable phase. Depending on the initial conditions, we find both long-lived cubic and tetragonal structures. At temperatures below $T\approx 70$ K, the tetragonal lattices prevail.

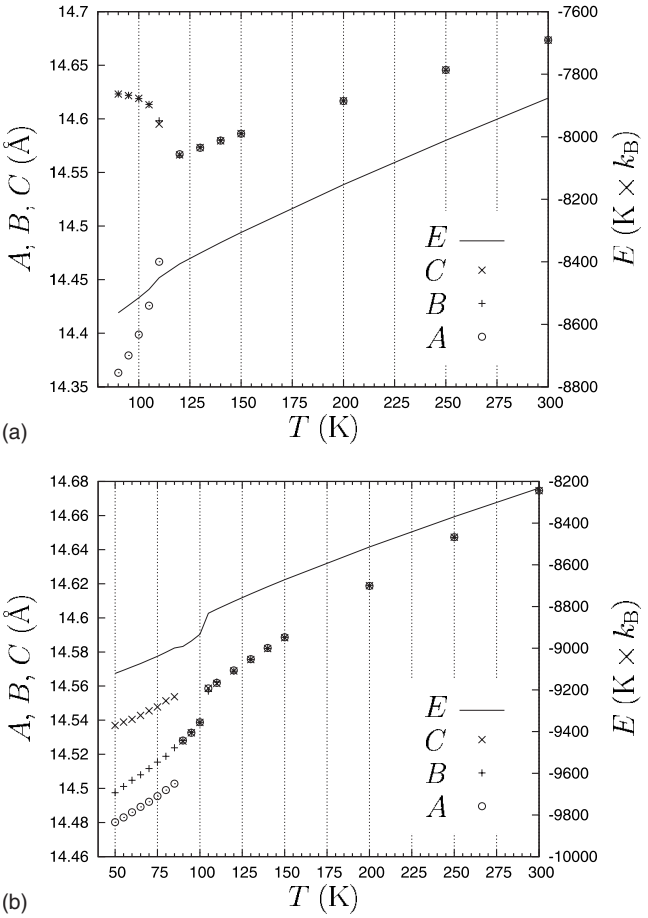

FIG. 6. Evolution of lattice constants (left abscissa, symbols) and energy (right abscissa, full line) as a function of temperature for (a) parameter set 1 and parameter set 2. Shown are averages over 10^5 MC steps.

For parameter set 2, Fig. 6(b), we also obtain a cubic phase at room temperature. Cooling down shows a jump in the energy and transition to a secondary cubic phase at $T_1 = 100$ K, which further transitions to an orthorhombic phase at $T_2 = 85$ K. The transition temperature T_2 displays a hysteresis; in our simulation, restarting at 85 K and slowly increasing to 90 K maintains an orthorhombic phase, while starting in the cubic phase at 90 K and cooling to 85 K preserves the cubic phase. The T_1 transition temperature is reproducible: cooling from $T=105$ to 100 K or heating from 100 to 105 K both result in the transition. The lattice constants of the orthorhombic phase lie very close together ($A=14.48$ Å, $B=14.50$ Å, and $C=14.54$ Å at 50 K). None of the parameter sets we tried resulted in values closer to the experimentally reported ones ($A=14.1$ Å, $B=14.6$ Å, and $C=15.3$ Å) at $T=105$ K.[2] However, we checked that the values truly split by examining the evolution of the lattice constants for all temperatures $T \leq 85$ K.

Comparing the two models, we observe higher densities and energies for parameter set 1 and that the cubic lattice constants above $T=105$ K coincide for the two potentials.

B. OMSDs

During the MC simulation, a sequence of orientations is generated for every C_{60} molecule. As the molecule adopts various orientations, any point $\vec{r}_i$ of the molecule, e.g., an atom or a bond (when speaking of a bond and its coordinates, the center of the bond is understood), results in a set of locations $\{\vec{r}_i(p), p=1,\ldots,N_{\mathrm{MC}}\}$, where i labels the C_{60} molecule, p labels subsequent MC steps, and N_{MC} is the total number of MC samples. The coordinates $\vec{r}_i=(x_i,y_i,z_i)$ of this "monitored" point are defined with respect to the local Cartesian system of axes (o,x,y,z). For a freely rotating molecule, the set $\{\vec{r}_i(p)\}$ eventually (for $N_{\mathrm{MC}}\to\infty$) covers a sphere with radius $R_i=|\vec{r}_i|$. If the molecule does not rotate at all, $\vec{r}_i$ remains constant. For the point $\vec{r}_i$ to be monitored, we choose a double bond of the C_{60} molecule. Although all 30 double bonds of a C_{60} molecule are equivalent, it is necessary to pick out one in particular. Let us choose double bond '1,' defined as the double bond with coordinates $\vec{r}_a = (0,0,z_a=3.48$ Å) when the C_{60} molecule is in the standard orientation [see Fig. 4(a)]. Apart from the monitored point $\vec{r}_i$, we select a reference point $\vec{r}_i^{\,0}$, again with respect to the local axis system (o,x,y,z). The average of the squared distances $u_i^2(p)=|\vec{r}_i(p)-\vec{r}_i^{\,0}|^2$ is then a measure for the degree of rotation. Well-chosen combinations of monitored and reference point lead to "OMSDs" quantifying molecular rotations.

For a first OMSD (labeled 'I'), we choose the point with coordinates $\vec{r}_a=(0,0,z_a)$ as the reference point $\vec{r}_i^{\,0}$. We stress that the reference point does not rotate along with the molecule; it remains fixed with respect to the molecule's center of mass. The associated OMSD reads as

$$\langle u_i^2\rangle_{\mathrm{MC}}^{\mathrm{I}} = \langle|\vec{r}_i(p)-\vec{r}_i^{\,0}|^2\rangle \equiv \frac{1}{N_{\mathrm{MC}}}\sum_{p=1}^{N_{\mathrm{MC}}}|\vec{r}_i(p)-\vec{r}_i^{\,0}|^2. \tag{4.1}$$

For a freely rotating molecule, the statistical OMSD [Eq. (4.1)] is given by

$$\langle u_i^2\rangle^{\mathrm{I}} = \frac{1}{4\pi}\int_0^{\pi}\sin\theta d\theta\int_0^{2\pi}d\phi|\vec{r}_i(\theta,\phi)-\vec{r}_i^{\,0}|^2, \tag{4.2}$$

where $\vec{r}_i(\theta,\phi)=(R\sin\theta\cos\phi, R\sin\theta\sin\phi, R\cos\theta)$ in spherical coordinates. For the present choice of reference and monitored point, one readily obtains the exact result

$$\langle u_i^2\rangle_{\mathrm{MC}}^{\mathrm{I}} = \langle u_i^2\rangle^{\mathrm{I}} = 2z_a^2 \quad \text{(free rotation)}. \tag{4.3}$$

On the other hand, for a nonrotating molecule, the monitored point $\vec{r}_i$ does not change during the simulation and the OMSD equals

$$\langle u_i^2\rangle_{\mathrm{MC}}^{\mathrm{I}} = |\vec{r}_i(p=1)-\vec{r}_i^{\,0}|^2 = \hat{u}_i^2 \quad \text{(no rotation)}. \tag{4.4}$$

The value $\hat{u}_i^2$ depends on the actual molecular orientation. Expression (4.4) in fact suggests a way to identify the molecular orientation. For example, when the C_{60} molecule adopts the standard orientation (and does not rotate), $\vec{r}_i(p=1)=\vec{r}_i^{\,0}$ and $\langle u_i^2\rangle_{\mathrm{MC}}^{\mathrm{I}}=0$ because of our choice of reference point and monitored point.

For a second OMSD (labeled 'II'), we choose the reference point to be the average of the monitored point: $\vec{r}_i^{\,0} = \langle\vec{r}_i\rangle_{\mathrm{MC}} = (1/N_{\mathrm{MC}})\Sigma_{p=1}^{N_{\mathrm{MC}}}\vec{r}_i(p)$. Obviously, for a nonrotating molecule $\vec{r}_i(p)\equiv\vec{r}_i$ is p-independent and $\langle\vec{r}_i\rangle=\vec{r}_i$ so that

$$\langle u_i^2\rangle_{\mathrm{MC}}^{\mathrm{II}} = 0 \quad \text{(no rotation)}. \tag{4.5}$$

For a freely rotating molecule, $\langle\vec{r}_i\rangle=\vec{0}$, so that

$$\langle u_i^2\rangle_{\mathrm{MC}}^{\mathrm{II}} = z_a^2 \quad \text{(free rotation)}. \tag{4.6}$$

There is a caveat concerning the selection of the monitored point. As mentioned above, at the very beginning of a simulation, all C_{60} molecules are put in the standard orientation [Fig. 4(a)] and double bond 1 has coordinates $(0,0,z_a)$. During the equilibration phase of the simulation, double bond 1 drifts away from its initial position. When calculating OMSDs, however, we want to trace the double bond closest to the location of double bond 1 in the standard orientation. Before starting a sequence of MC steps to calculate MC averages of OMSDs, we therefore determine which of the 30 double bonds lies closest to $(0,0,z_a)$ and "mark" it as the point to be monitored. This synchronizing step is of crucial importance to take the high molecular symmetry into account. Indeed, without it, different realizations of a same molecular orientation—we point out that the icosahedral group I_h contains 120 symmetry operations—would result in different $\langle u_i^2\rangle_{\mathrm{MC}}$ values, making the identification of equivalent molecular orientations extremely complicated.

The pattern of numbers following from Eqs. (4.3)–(4.6) allows an analysis of the molecular rotations and even a determination of the molecular orientations in the case of nonrotating molecules. Indeed, if we obtain $\langle u_i^2\rangle_{\mathrm{MC}}^{\mathrm{I}}=2z_a^2=24.22$ Å^2 and $\langle u_i^2\rangle_{\mathrm{MC}}^{\mathrm{II}}=z_a^2=12.11$ Å^2, the molecules rotate freely. If we obtain $\langle u_i^2\rangle_{\mathrm{MC}}^{\mathrm{II}}=0$, we can conclude that the molecules are orientationally frozen. In Figs. 7(a) and 7(b) we show $\langle u_i^2\rangle_{\mathrm{MC}}^{\mathrm{I}}$ and $\langle u_i^2\rangle_{\mathrm{MC}}^{\mathrm{II}}$, averaged over all 500 molecules, for potential parameter sets 1 and 2. Clearly, at room temperature, the C_{60} molecules rotate freely for both potential models. At about 100 K, the OMSD values start to decrease as orientational freezing sets in. In all our simulations with

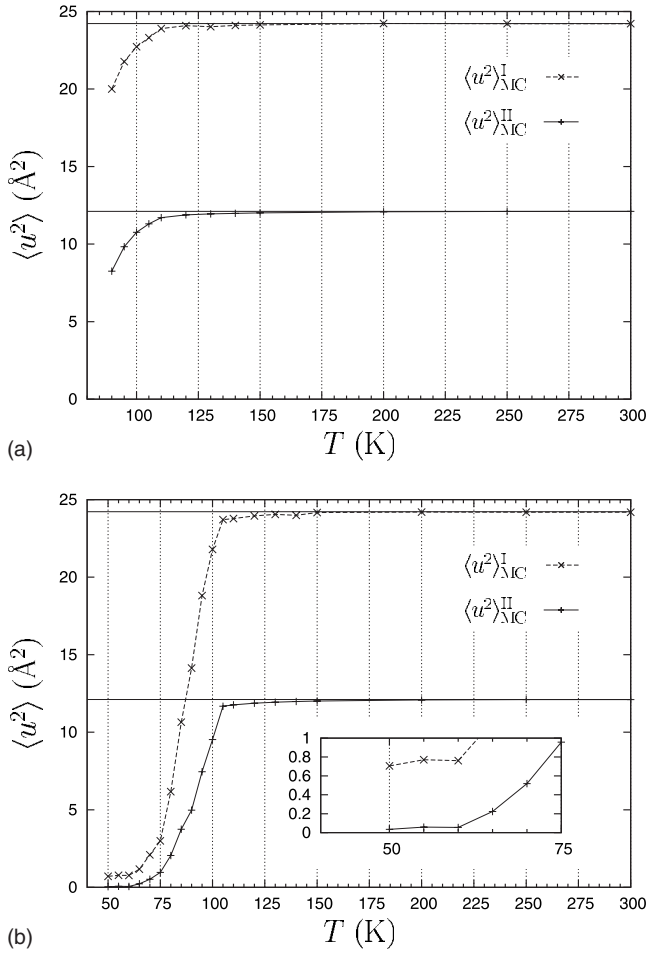

FIG. 7. OMSD values I and II for the C_{60} molecules as a function of temperature, obtained by averaging 25 000 MC steps over all 500 molecules in the simulation box. The free-rotation values $2z_a^2=24.22$ Å^2 and $z_a^2=12.11$ Å^2 are shown as horizontal lines. (a) Potential parameter set 1. (b) Potential parameter set 2.

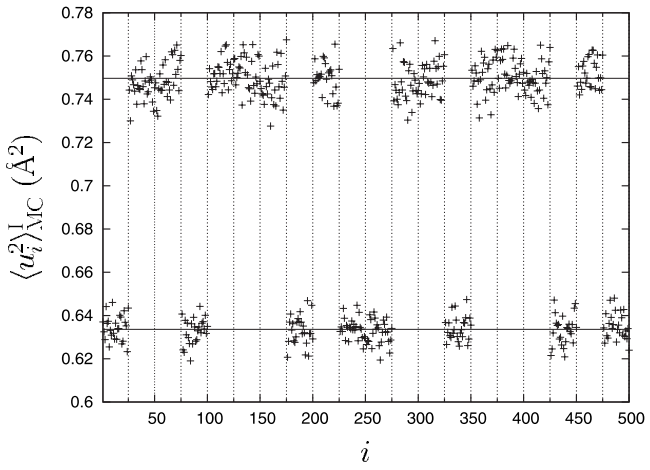

FIG. 8. OMSD value $\langle u_i^2\rangle^{\mathrm{I}}_{\mathrm{MC}}$ plotted per C_{60} molecule (parameter set 2), averaged over 2500 MC steps. Fluctuations around two distinct values can be clearly seen.

set 1, both OMSD I and II start to decrease smoothly around 110 K and are close to zero (<0.4 Å^2) at 50 K. The transition from free rotation to fixed orientations covers the range of 65 K$\lesssim T\lesssim$110 K. However, we recall that the low-T thermodynamically stable phase is not evident for model 1; caution is therefore required when interpreting the $\langle u^2\rangle$ values. By means of molecular dynamics, where time scales can be explicitly assessed, Coluci *et al.*[44] found at 200 and 400 K ballistically free rotation of the C_{60} molecules at short times ($\lesssim$1 ps), librations at intermediate, and rotational diffusion at longer times ($\gtrsim$10 ps). The long-time rotational diffusion in Ref. 44 corresponds to the (diffusive) free rotations observed in our MC simulations at temperatures larger than about 110 K.

At 50 K, for parameter set 2, the value of $\langle u_i^2\rangle^{\mathrm{II}}_{\mathrm{MC}}$ is close to zero ($\langle u_i^2\rangle^{\mathrm{II}}_{\mathrm{MC}}=0.035$ Å^2). This value can be interpreted as resulting from small rotational fluctuations around a fixed orientation. The value of $\langle u_i^2\rangle^{\mathrm{I}}_{\mathrm{MC}}=0.706$ Å^2 is different from zero, however, implying that the molecules are not in the standard orientation. First, we make a plot of the $\langle u_i^2\rangle^{\mathrm{I}}_{\mathrm{MC}}$ value per molecule; the result is shown in Fig. 8. Two subsets of molecules can be distinguished: one with $\langle u_i^2\rangle^{\mathrm{I}}_{\mathrm{MC}}=u_A^2=0.749$ Å^2 and one with $\langle u_i^2\rangle^{\mathrm{I}}_{\mathrm{MC}}=u_B^2=0.633$ Å^2. These two values correspond to two classes of orientations. In Fig. 8, one sees that the $\langle u_i^2\rangle^{\mathrm{I}}_{\mathrm{MC}}$ values within subsequent groups of 25 molecules ($i=1,\ldots,25$, $i=26,\ldots,50$, etc.) are nearly equal. Considering the construction of our $5\times5\times5$ simulation box, it follows that each of these groups corresponds to a set of 25 molecules within a plane parallel to the (Y,Z)-plane; the molecules in such a plane have their n_1 value in common—we recall that equilibrium lattice positions of the C_{60} molecules read as $\vec{X}=n_1\vec{A}+n_2\vec{B}+n_3\vec{C}$.

Having established the presence of two different classes of molecular orientations and an ordering pattern connected to planes of molecules parallel to the $(\vec{B},\vec{C})$-plane, we proceed with characterizing and visualizing the orientations of the groups of 25 molecules. We focus on a presentation of the general outcome. Full details are given in the Appendix. For each of the two classes ("families," labeled A and B) corresponding to the values u_A^2 and u_B^2, we recover four different orientations ("members," labeled 1, 2, 3, and 4). The sequence of 20 groups each containing 25 molecules oriented in the same way can be seen as a $5\times1\times1$ supercell and our simulation box (omitting the cubane molecules) as the repetition along the $\vec{B}$ and $\vec{C}$ axes of supercell, which is shown schematically as in Fig. 9(a) with labeled spheres representing the C_{60} molecules and their orientations. To each of the molecules in the supercell, we have attributed Euler angles (α,β,γ). The associated Euler rotations (starting from the standard orientation) transform the molecules to their respective orientations—for details, we refer to the Appendix. In Fig. 9(b) we show the $5\times1\times1$ supercell with the C_{60} molecules in their actual orientations.

Figure 9(b) shows that families A and B hardly differ from each other: $A_1\approx B_1$, $A_2\approx B_2$, $A_3\approx B_3$, and $A_4\approx B_4$. This can be clearly seen in Fig. 10(a) where we show the projection on the (X,Z)-plane of the eight far right C_{60} molecules of Fig. 9—in this subset of eight molecules, all eight different orientations occur once. Furthermore, the orientations bear a striking resemblance to the orientations of the C_{60} molecules in fullerite; the projection on the (X,Z)-plane of the fcc unit cell of C_{60} fullerite is shown in Fig. 10(b).[45]

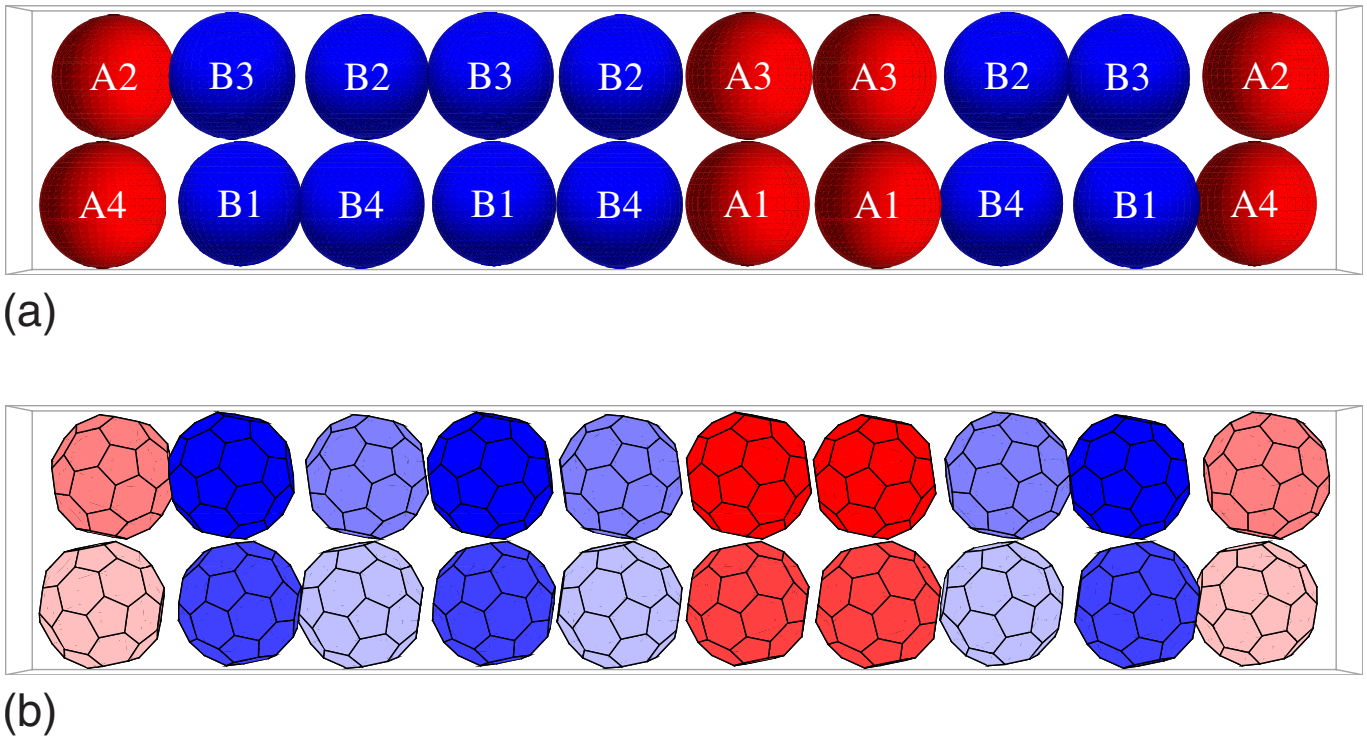

FIG. 9. (Color online) (a) Visualization of the $5\times1\times1$ supercell showing the occurrence of eight different orientations of C_{60} molecules (represented as spheres). The labels stand for molecular orientations. (b) Schematic visualization of the $5\times1\times1$ supercell showing the low-T orientational pattern of the C_{60} molecules.

While it is tempting to attribute the small differences between A_1 and B_1, etc., to thermal fluctuations and to claim that the realistic structure is the one with only four sublattices with different orientations as in C_{60} fullerite at low temperature, our orientational analysis outlined in the Appendix shows that the averages over many independent configurations indeed result in two times four orientational sublattices. Both families are small deviations from the low-T fcc arrangement of C_{60} molecules in fullerite.

It is interesting to note that we recover one of the low-T C_{60} fullerite orientations as the lowest-energy orientation of a C_{60} molecule in our parameter set 2 orthorhombic phase when considering the interaction with its six nearest cubane neighbors only (Fig. 11). Because the optimal structure without cubane molecules (fullerite) preserves this orientation, i.e., results from $C_{60}-C_{60}$ interactions in a *cubic* lattice, the deviations seen in the actual orientations of fullerene-cubane's orthorhombic phase seem to be the result of the

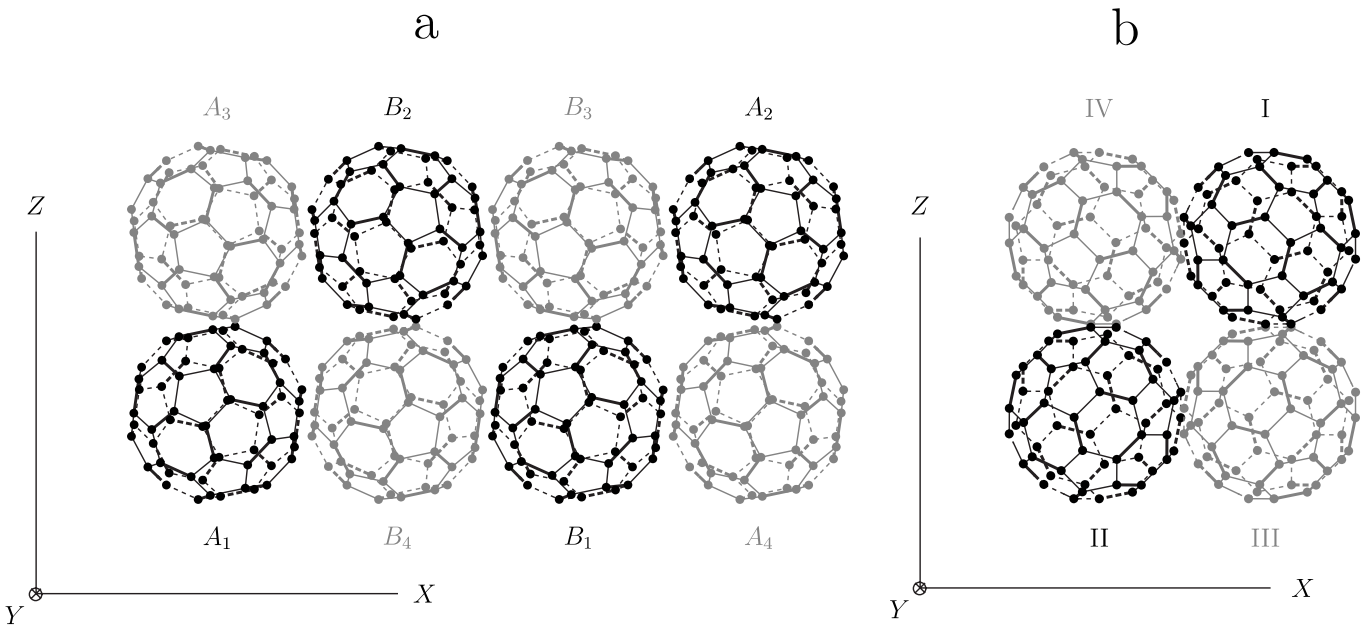

FIG. 10. (a) The far right 8 C_{60} molecules in Fig. 9, compared to (b) the $Pa\bar{3}$ unit cell of C_{60} fullerite.

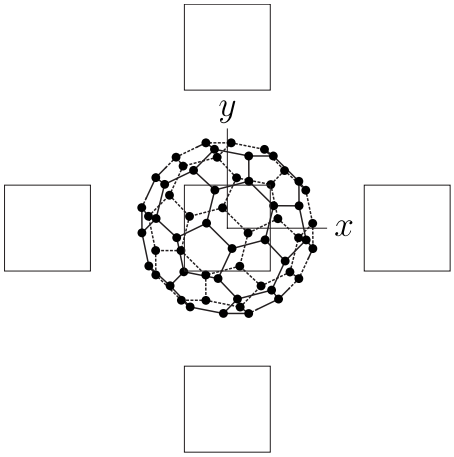

FIG. 11. Lowest-energy orientation of a C_{60} molecule in an environment of six cubane molecules, schematically shown as squares (orthorhombic phase, parameter set 2, $T=50$ K). This orientation is the same as orientation I in Fig. 2(b).

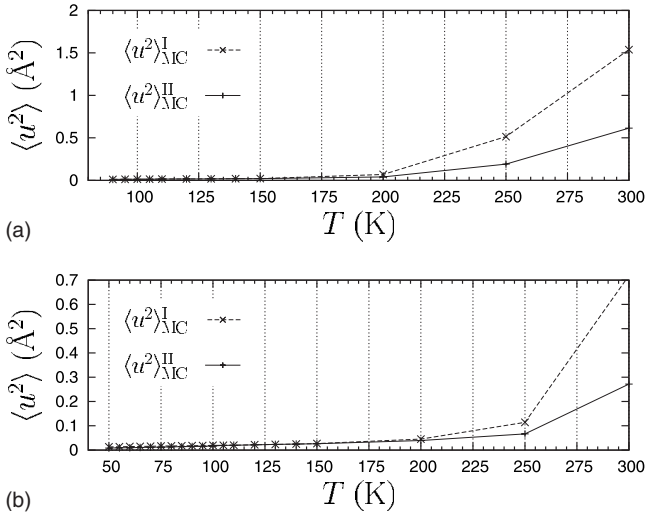

FIG. 12. OMSD values I and II for the C_8H_8 molecules, as a function of temperature. Obtained by averaging over 25 000 MC steps and over all molecules in the simulation box. (a) Potential parameter set 1; free-rotation values $2z_b^2=2.409$ Å^2 and $z_b^2=1.205$ Å^2. (b) Potential parameter set 2; free-rotation values $2z_b^2=3.998$ Å^2 and $z_b^2=2.000$ Å^2.

symmetry lowering of the crystal lattice (cubic-to-orthorhombic) induced by the cubane molecules. The occurrence of two slightly differing families of molecular orientations can be interpreted as orientational frustration; no single set of four orientations minimizes the free energy, but two sets of four orientations do.

We note that the very development of the pattern of orientations visualized in Fig. 9 at 50 K indicates that any possible biasing effects due to the highly ordered starting configuration (all C_{60} molecules in the standard orientation) have disappeared during equilibration.

The concept of OMSDs is easily applied to the C_8H_8 molecules as well. For monitored and reference points we have chosen faces of the cubes; they are represented by the coordinates of their midpoints. We set up two OMSDs analogous to those for the C_{60} molecules. The monitored point is the face with coordinates $(0,0,z_b>0)$ when the C_8H_8 molecule is in its standard orientation [Fig. 4(b)]. For the first OMSD, the reference point is the point $\vec{r}_b=(0,0,z_b)$. For the second, the reference point is the average of the monitored point. The resulting values, averaged over all 500 cubane molecules, are plotted in Fig. 12. Clearly, for both potential parameter sets, at low temperature, the cubane molecules do not rotate: $\langle u_i^2\rangle^{\rm II}_{\rm MC}=0$. The value $\langle u_i^2\rangle^{\rm I}_{\rm MC}$ is extremely close to zero [0.007 Å^2 and 0.013 Å^2 for sets 1 (90 K) and 2 (50 K), respectively], from which we conclude that the low-T orientation is the standard orientation. At room temperature, OMSDs I and II are nonzero, but smaller than the respective free-rotation values $2z_b^2$ and z_b^2, as seen in Figs. 12(a) and 12(b). (Note that the value of z_b is different for parameter sets 1 and 2: $z_b=1.098$ Å and 1.414 Å, respectively.) The deviation at $T\geq 250$ K from the linear trend present for $T\leq 200$ K is due to the reorientations of the cubane molecules. When we examine the MC averages of the coordinates of the monitored point at 300 K for each molecule separately, we see that several molecules have values approximately equal to $(0,0,z_b)$. The other molecules have undergone at least one flip to another orientation. This orientation is likely to be equivalent to the standard orientation, however, but introduces a bias in the average since the distance squared between monitored and reference bond now systematically lies around another value. For longer simulation runs, the number of flipped cubanes increases: for parameter set 2 at 300 K, $\langle u_i^2\rangle^{\rm I}_{\rm MC}=0.298$ Å^2 for 5000 MC steps, while for 25 000 steps this value has increased to 0.718 Å^2.

V. *NVT*-ENSEMBLE SIMULATIONS

After *NpT*-simulations we performed *NVT*-runs; for each temperature we simply took a *NpT*-configuration as the starting point. In *NVT*-ensemble we sampled pair distribution functions and translational mean-squared displacements.

A. Pair distribution functions

The pair distribution function $g(r)$ expresses the (relative) probability of finding two molecules at a distance r apart. Since we have two types of molecules, we can construct four pair distribution functions: $g_{aa}(r)$, $g_{bb}(r)$, and $g_{ab}(r)=g_{ba}(r)$. Here, $g_{aa}(r)$ refers to $C_{60}-C_{60}$ distances, $g_{ab}(r)=g_{ba}(r)$ to $C_{60}-C_8H_8$ distances, and $g_{bb}(r)$ to $C_8H_8-C_8H_8$ distances. These functions can be easily sampled in a *NVT*-simulation (see, e.g., Ref. 30). In Fig. 13 we show $g_{aa}(r)$ and $g_{bb}(r)$ for both parameter set 2 at low and high T (50 and 300 K). Distances have been measured from the molecules' centers of mass.

The peak positions reflect the crystal lattice. The high-T fcc phase [Fig. 13(b)] is characterized by peaks at the lattice neighbor-distances $1/\sqrt{2}a, a, \sqrt{6}/2a, \sqrt{2}a, \ldots$. For the orthorhombic low-T phase, the peaks seen in the high-T cubic phase split into three; however, these splits cannot be resolved in the plots presented here since the values of the lattice constants lie very close to each other.

The comparison of the peak widths and heights of $g_{aa}(r)$ and $g_{bb}(r)$ shows that $g_{aa}(r)$ has higher and narrower peaks than $g_{bb}(r)$. This is a consequence of the cubane molecules'

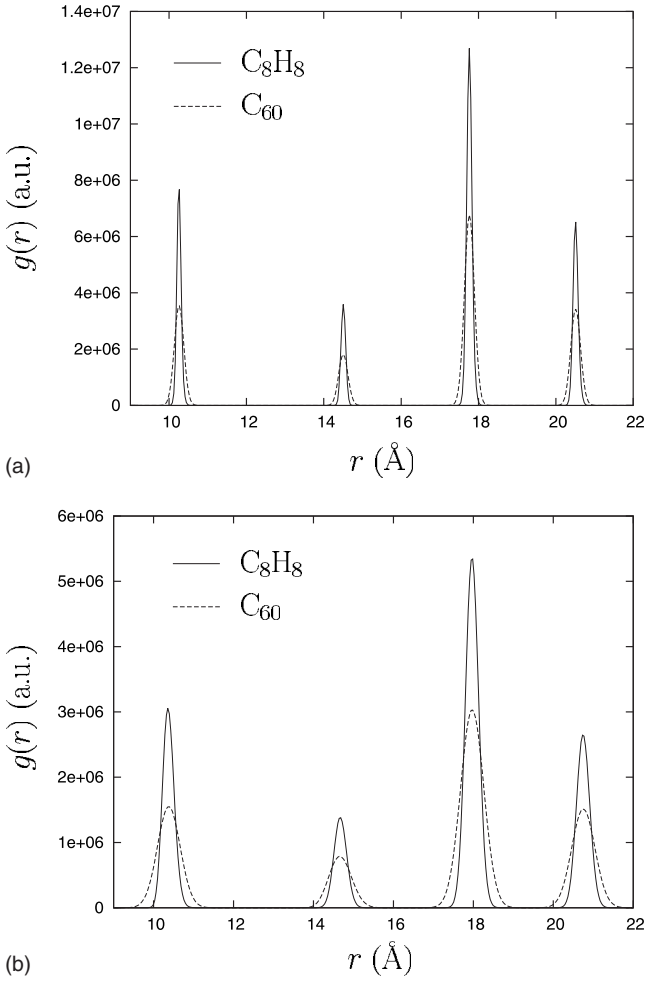

FIG. 13. Pair distribution functions $g_{aa}(r)$ (solid line) and $g_{bb}(r)$ (dashed line) for parameter set 2 at (a) $T=50$ K and (b) $T=300$ K. The differences in lattice constants of the orthorhombic phase (b) are too small to result in discernable peak splitting. For the MC average, 5000 samples were taken.

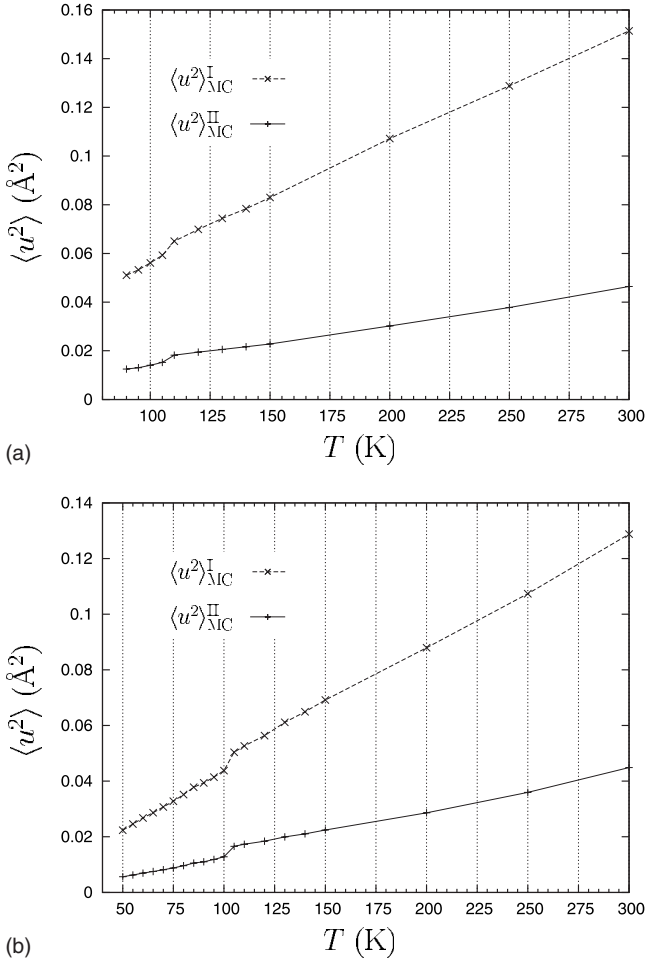

FIG. 14. Translational mean-squared displacements $\langle u_i^2\rangle_{\mathrm{MC}}$ for (a) potential parameter set 1 and (b) potential parameter set 2. For both sets, the cubane molecules (dashed lines) display larger thermal fluctuations than the fullerene molecules (solid lines). For the MC average, 5000 samples were taken.

larger translational mobility than that of the fullerene molecules. Obviously, the broader peaks at higher T in both $g_{aa}(r)$ and $g_{bb}(r)$ are due to larger thermal fluctuations.

B. Translational mean-squared displacements

Analogous to the OMSDs introduced in Sec. IV B, we sampled translational mean-squared displacements given by

$$\langle u_i^2\rangle_{\mathrm{MC}} = \langle|\vec{\tilde{r}}_i(p) - \langle\vec{\tilde{r}}_i\rangle|^2\rangle, \tag{5.1a}$$

$$\vec{\tilde{r}}_i(p) = \vec{r}_i(p) - \vec{M}(p), \tag{5.1b}$$

with $\vec{M}(p)=(1/N)\Sigma_{i=1}^{N}\vec{r}_i(p)$ the center of mass of the N molecules in the simulation box. This definition takes a drift of the simulation box into account.

We sampled fullerene and cubane translations; in Fig. 14 we show the resulting values of $\langle u_i^2\rangle_{\mathrm{MC}}$, averaged over all 500 molecules, for our two parameter sets. Two conclusions can be drawn: (1) there is a linear decrease in mean-squared displacements with decreasing temperature, with a jump, and a change in slope at the transition temperature, and (2) at a given temperature, the cubane molecules display larger mean-squared displacements. The latter can be ascribed to the larger spatial freedom of the cubes in the octahedral voids. Indeed, the C_{60} molecules are already translationally confined by their own sublattice, while the C_8H_8 molecules have some excess space available. Note that this observation is consistent with the broader peaks in $g_{bb}(r)$ compared to $g_{aa}(r)$ as mentioned above. We also point out the generally larger translational mean-squared displacements for model 1 due to the smaller cube size for modeling C_8H_8 molecules.

VI. DISCUSSION AND CONCLUSIONS

The heteromolecular crystal $C_{60}\cdot C_8H_8$ (fullerene-cubane), a mixture of icosahedrally and cubically shaped molecules with 1:1 stoichiometry, undergoes a structural phase transition upon cooling:[1] at $T_c\approx 140$ K, the crystal structure changes from cubic (space group $Fm\bar{3}m$) to orthorhombic. The lattice change is accompanied by rotational freezing of the C_{60} molecules.

In order to provide more insight in the low-T structure of fullerene-cubane, we performed MC simulations with particular attention to the description of molecular orientational properties. The key component of our MC simulation program is the potential model for calculating intermolecular

interactions. We have used a simple model based on LJ pair interactions with a limited number of potential constants capturing the specific symmetries of the C_{60} and the C_8H_8 molecules. From the vast number of possible parameter sets, we retained two models differing in the interaction strength between and the size of the cubane molecules.

Our simulations at constant pressure (*NpT*-ensemble) reveal a structural phase transition for both potential models. The first parameter set results in a cubic-to-tetragonal transition at about $T=110$ K [Fig. 6(a)]. Parameter set 2 is the preferred model since it results in an orthorhombic state at low temperature [Fig. 6(b)], in agreement with experiment.[1,2] Upon cooling from room temperature, a cubic-to-cubic transition takes place at $T_1 \approx 105$ K; the orthorhombic phase sets in at around $T_2 \approx 85$ K. A hysteresis around T_2 is observed. Potential model 2 may therefore be considered a satisfactory model offering computational simplicity while capturing the essential physical behavior.

In order to investigate the molecule's orientational motion, we introduced OMSDs. The idea is to choose a monitored point, rotating along with the molecule, and a fixed reference point and measure the distance (squared) between them. This approach not only allows a quantification of the "degree of rotation" and a determination of the actual orientations of rotationally frozen molecules but is also efficient from a data-storage point of view: only the coordinates of two monitored points have to be stored for each molecule. In agreement with experiment,[1] the cubane molecules adopt fixed orientations, with their faces parallel to the crystal axes [Fig. 4(b)], at both low and high temperature, for both parameter sets. Thermal orientational fluctuations increase with temperature. For the C_{60} molecules, we see a continuous transition from free rotation at room temperature to fixed orientations at 50 K. A broad transition range is seen: down to $T \approx 105$ K, the molecules rotate freely or quasifreely, at $T \approx 75$ K (parameter set 2), molecules get settled in specific orientations. This is similar to the transition in C_{60} fullerite: ^{13}C NMR measurements show a slowing down of the rotational motion of the C_{60} molecules with decreasing temperature.[14]

With parameter set 2, we observe the development at $T=50$ K of eight groups of molecules having the same orientation. The resulting structure can be described by a unit cell of dimensions $5A$, B, and C. The molecule's orientations in the unit cell, shown in Fig. 9 with the cubane molecules omitted, can be classified into two families (A and B), each having four members (A_1, A_2, etc.). The corresponding orientations of the two families (A_1 and B_1, A_2 and B_2, etc.) are only slightly different, and the arrangement of molecules is very similar to the pattern of orientations observed in C_{60} fullerite at low temperature (see Fig. 10). In C_{60} fullerite, four sublattices of C_{60} molecules each with a different orientation occur; the four different orientations are obtained by starting from the standard orientation and rotating over 22.0° about the local (normalized) $[uuu]$, $[u\bar{u}\bar{u}]$, $[\bar{u}u\bar{u}]$, and $[\bar{u}\bar{u}u]$ vectors, with $u=1/\sqrt{3}=0.577$. The A orientations are obtained by similar rotations over 21.9° about vectors slightly differing from $[uuu]$, $[u\bar{u}\bar{u}]$, $[\bar{u}u\bar{u}]$, and $[\bar{u}\bar{u}u]$; the B orientations by rotating over 22.8° about vectors close to the A vectors. Both orientational sets A and B deviate very little from the ideal $Pa\bar{3}$ space group where a pentagon of one C_{60} molecule faces a double bond of a neighboring molecule. Recalling the presumption in the experimental work of Pekker *et al.*[1] of a doubling of the periodicity along one of the crystal axes in the orthorhombic phase, we realize that a possible periodicity doubling mechanism is provided by the alternation of A and B orientational patterns. For example, considering the eight molecules shown in Fig. 10(a) as the unit cell (omitting the cubane molecules) would imply a doubled periodicity along the $\vec{A}$-direction. In view of the small differences between the two orientational families A and B, the corresponding superstructure might be not easily resolvable in a (powder) diffraction experiment and difficult to determine. In the case of the doubled unit cell [Fig. 10(a)], the $(5\vec{A},\vec{B},\vec{C})$ supercell in Fig. 9 displays some defects, however. Starting from the left, the first four B orientations are followed by another set of four B orientations. A second defect is the repetition of A_1A_3 at $\vec{X}=3\vec{A}$ after $\vec{X}=2.5\vec{A}$, compensated by the defect at the edge of the supercell (A_4A_2 at both $n_1=4.5$ and $n_1=0$). It is likely that these defects are due to finite-size effects of our simulation setup; a doubled unit cell is incompatible with a simulation box built up from an odd number of unit cells along each direction. Orientational stacking faults as detected here are in reality certainly possible since they would result in only small (free) energy surpluses because of the slight differences between the A and B orientations but they would probably occur with a much lower density.

Translational motion of the molecules was investigated by performing runs in *NVT*-ensemble. Next to observing an overall linear increase in mean-squared displacements with increasing temperature, we were able to conclude that the C_8H_8 molecules display larger displacive fluctuations due to the relatively large available interstitial space formed by the surrounding C_{60} molecules.

It turns out that our results, qualitatively of high importance in understanding the structural features of fullerene-cubane, quantitatively manifest themselves rather weakly. The orthorhombic lattice constants, while clearly separated, lie close together, and orientational differences, while providing an explanation for a possible superstructure, are minimal. We believe that this might be due to the simplicity of our potential model and very difficult to fix by adjusting potential parameters. The reduction in a cubane molecule to a cube is drastic and could be the origin of an oversimplification of our intermolecular potential model. For future simulations, it might be worthwhile to invest in a more accurate description of the cubane molecule, the obvious first step being to consider both C and H atoms as interaction centers.

We are convinced that the insights provided by our simulations are useful for understanding past[1,2,5] and ongoing[11] x-ray diffraction work and that they can serve as starting points for MC simulation studies of related systems.

ACKNOWLEDGMENTS

The authors thank P. Launois, J. Cambedouzou, and K. H. Michel for several helpful discussions. B.V. acknowledges the Research Foundation-Flanders (FWO-Vl) for a Mobility Grant for his stay at the Institut für Festkörperforschung, Forschungszentrum Jülïch. B.V. is a Postdoctoral Fellow of the Research Foundation-Flanders (FWO-Vl).

APPENDIX: MOLECULAR ORIENTATIONS

Here we describe in more detail our procedure to obtain the precise orientations of the C_{60} molecules resulting from the MC simulations with parameter set 2 at $T=50$ K.

Our starting point is the observation of two classes of orientations, manifested by fluctuations of the OMSD $\langle u_i^2\rangle_{\mathrm{MC}}^{\mathrm{I}}$ around two distinct average values ($u_A^2=0.749$ Å^2 and $u_B^2=0.633$ Å^2), as seen in Fig. 8. It is incorrect to *a priori* claim that all molecules with the same OMSD value (u_A^2 or u_B^2) have the same orientation since the value $\langle u_i^2\rangle_{\mathrm{MC}}^{\mathrm{I}}$ does not completely define a molecule's orientation. Indeed, both a rotation about the local z-axis and a rotation about the vector connecting the local origin o and the monitored point $\vec{r}_1^{\,i}=(x_1^i,y_1^i,z_1^i)$ leave the value of $\langle u_i^2\rangle_{\mathrm{MC}}^{\mathrm{I}}=(x_1^i)^2+(y_1^i)^2+(z_1^i-z_a)^2=R^2-z_1^i z_a+z_a^2$ invariant—the former does not affect z_1^i, while the latter does not affect (x_1^i,y_1^i,z_1^i). Here we have introduced the subscript 1 to denote the monitored point considered in Sec. V—the double bond closest to $(0,0,z_a)$. Considering the coordinates x_1^i, y_1^i, and z_1^i of the monitored point as indicators for the molecule's orientation instead of only its distance (squared) to the z-axis rules out a rotation about the z-axis, but a rotation about $o\vec{r}_1^{\,i}$ then still leaves the coordinates of the monitored point invariant. We therefore introduced a second monitored point, $\vec{r}_2^{\,i}=(x_2^i,y_2^i,z_2^i)$: the double bond with coordinates $(z_a,0,0)$ when the C_{60} molecule is in the standard orientation. Synchronization was applied for this point as for $\vec{r}_1^{\,i}$, the double bond closest to $(z_a,0,0)$ was located and marked the before sampling. The set of coordinates $\{x_1^i,y_1^i,z_1^i,x_2^i,y_2^i,z_2^i\}$ fixes the molecule's orientation completely. Mathematically, the failure of $\langle u_i^2\rangle_{\mathrm{MC}}^{\mathrm{I}}$ or (x_1^i,y_1^i,z_1^i) to completely determine the molecular orientation lies in the need for three independent parameters to do so. The value $\langle u_i^2\rangle_{\mathrm{MC}}^{\mathrm{I}}$ is simply not sufficient, and the three coordinates x_1^i, y_1^i, and z_1^i are not independent since $(x_1^i)^2+(y_1^i)^2+(z_1^i)^2=R^2$. On the other hand, the set $\{x_1^i,y_1^i,z_1^i,x_2^i,y_2^i,z_2^i\}$ contains redundancy. However, it is instructive to consider all six coordinates. In Fig. 15 we show the values of x_1^i and y_1^i per molecule, averaged over the same 5000 MC steps as for $\langle u_i^2\rangle_{\mathrm{MC}}^{\mathrm{I}}$ in Fig. 8. For all six coordinates, patterns of the same groups of 25 molecules as for $\langle u_i^2\rangle_{\mathrm{MC}}^{\mathrm{I}}$ are clearly distinguishable. The order contained within these patterns is striking: not a single deviation from the groups of 25 molecules is seen. In view of the large number of MC steps, this ordering demonstrates beyond doubt the presence of particular molecular orientations. Analyzing the plots of the coordinates $\{x_1^i,y_1^i,z_1^i,x_2^i,y_2^i,z_2^i\}$ reveals the existence of eight different orientations. This can be seen, for example, by starting with the plot of y_1^i, already displaying four different values (orientations), and then considering the plot of x_1^i, which doubles the number of orientations. We introduce the notations A and B for two families of orientations, each consisting of four members labeled 1, 2, 3, and 4. The eight different orientations are then symbolized as A_1, A_2, A_3, A_4, B_1, B_2, B_3, and B_4. The groups of 25 molecules each correspond to layers of molecules parallel to the crystallographic $(\vec{B},\vec{C})$-plane. Due to the layout of our simulation box (composed of $5\times5\times5$ face-centered, originally cubic, cells), we have two layers per n_1 value, where n_1 specifies the location of the molecule (group of molecules) along the $\vec{A}$ direction. The equilibrium lattice position of the C_{60} molecules read $\vec{X}=n_1\vec{A}+n_2\vec{B}+n_3\vec{C}$; the 500 molecules in our simulation box are distributed according to

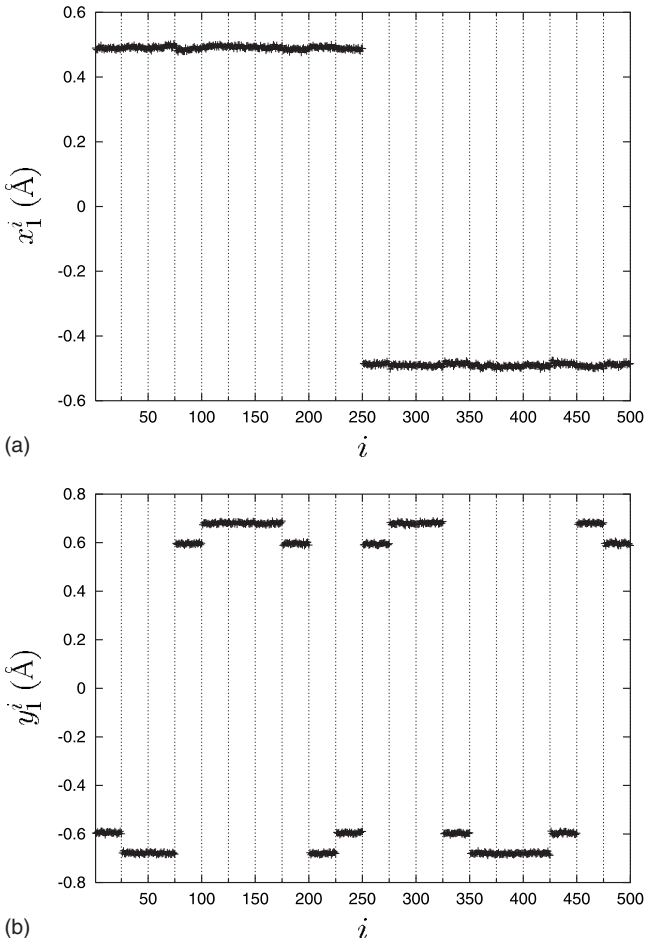

FIG. 15. Values of the coordinates of the monitored points x_1^i and y_1^i, plotted per C_{60} molecule (labeled $i=1,\ldots,500$). Parameter set 2, $T=50$ K.

$$\{\vec{X}_i, i=1,\ldots,125\}=m_1\vec{A}+m_2\vec{B}+m_3\vec{C} \quad \text{with} \quad i=25m_1+5m_2+m_3, \tag{A1a}$$

$$\{\vec{X}_i, i=126,\ldots,250\}=m_1\vec{A}+m_2\vec{B}+m_3\vec{C} \quad \text{with} \quad i=25m_1+5m_2+m_3+125, \tag{A1b}$$

$$\{\vec{X}_i, i=251,\ldots,375\}=m_1\vec{A}+m_2\vec{B}+m_3\vec{C} \quad \text{with} \quad i=25m_1+5m_2+m_3+250, \tag{A1c}$$

TABLE II. Euler angles (α,β,γ), unnormalized rotation vector $\tilde{\vec{p}}=(\tilde{p}_1,\tilde{p}_2,\tilde{p}_3)$, and rotation angle ϕ for each of the eight molecular orientations in the $5\times1\times1$ supercell in Fig. 9.

	α	β	γ	$\tilde{p}_1$	$\tilde{p}_2$	$\tilde{p}_3$	ϕ (deg)
A_1	1.690 437	1.374 923	3.476 121	0.654 460	−0.527 026	−0.542 149	21.915 183
A_2	1.451 639	1.374 500	5.947 850	0.654 767	0.526 577	0.542 214	21.942 513
A_3	4.832 304	1.374 947	0.334 793	−0.654 546	0.527 100	−0.541 974	21.930 997
A_4	4.593 200	1.374 384	2.807 012	−0.654 426	−0.526 727	0.542 481	21.924 809
B_1	1.713 637	1.365 455	3.469 338	0.647 169	−0.537 345	−0.540 770	22.812 320
B_2	1.427 886	1.365 641	5.955 616	0.647 123	0.537 441	0.540 730	22.801 377
B_3	4.855 351	1.365 484	0.327 525	−0.647 069	0.537 447	−0.540 789	22.808 023
B_4	4.569 585	1.365 804	2.813 992	−0.647 180	−0.537 413	0.540 690	22.792 382

$$\{\vec{X}_i, i=376,\ldots,500\}=m_1\vec{A}+m_2\vec{B}+m_3\vec{C} \quad \text{with } i=25m_1+5m_2+m_3+375 \tag{A1d}$$

with $m_1,m_2,m_3=0,\ldots,4$. The whole simulation box can therefore be described by a $5\times1\times1$ supercell, repeated five times along $\vec{B}$ and five times along $\vec{C}$. In Fig. 9(a) the $5\times1\times1$ supercell is schematically shown with labeled balls representing the C_{60} molecules in their respective orientations.

The next step is to visualize and understand the actual molecular orientations symbolized by $A_1,\ldots,B_4$. First, we average the coordinates $\{x_1^i,y_1^i,z_1^i,x_2^i,y_2^i,z_2^i\}$ within each group of 25 molecules, resulting in 20 sets $\{\bar{x}_1^j,\bar{y}_1^j,\bar{z}_1^j,\bar{x}_2^j,\bar{y}_2^j,\bar{z}_2^j\}$, $j=1,\ldots,20$, with

$$\bar{x}_1^j=\frac{1}{25}\sum_{t=1}^{25}x_1^i|_{i=25(j-1)+t} \tag{A2}$$

and likewise for $\bar{y}_1^j,\ldots,\bar{z}_2^j$. For characterizing the molecule's orientation, the three Euler angles are most adequate. We use the convention in Ref. 46: the three Euler rotations are (i) a rotation over $0\le\alpha<2\pi$ about the z-axis, followed by (ii) a rotation over $0\le\beta\le\pi$ about the y-axis, and finally (iii) a rotation over $0\le\gamma<2\pi$ about the z-axis again. The x-, y- and z-axes are kept fixed. The point with coordinates $\vec{r}$ is then transformed to $\vec{r}\,'=\mathfrak{R}_{zyz}(\alpha,\beta,\gamma)\vec{r}=\mathfrak{R}_z(\gamma)\mathfrak{R}_y(\beta)\mathfrak{R}_z(\alpha)\vec{r}$, where $\mathfrak{R}_z(\alpha)$, $\mathfrak{R}_y(\beta)$, and $\mathfrak{R}_z(\gamma)$ are the rotation matrices of the corresponding Euler rotations. To match the set $\{\bar{x}_1^j,\bar{y}_1^j,\bar{z}_1^j,\bar{x}_2^j,\bar{y}_2^j,\bar{z}_2^j\}$ to Euler angles $(\alpha_j,\beta_j,\gamma_j)$ we set up a least-squares fit; we minimize the function

$$f_j=(z_1'-\bar{z}_1^j)^2+(x_2'-\bar{x}_2^j)^2+(z_2'-\bar{z}_2^j)^2 \tag{A3}$$

with respect to α, β, and γ. In Eq. (A3), z_1' stands for the z-coordinate of the double bond closest to $(0,0,z_a)$ after application of the rotation operator $\mathfrak{R}_{zyz}(\alpha,\beta,\gamma)$, x_2' stands for the x-coordinate of the double bond closest to $(z_a,0,0)$ after application of the rotation operator $\mathfrak{R}_{zyz}(\alpha,\beta,\gamma)$, and z_2' stands for the z-coordinate of the double bond closest to $(z_a,0,0)$ after application of the rotation operator $\mathfrak{R}_{zyz}(\alpha,\beta,\gamma)$—definitions taking the synchronization procedure into account. Note that $\bar{x}_1^j$, $\bar{y}_1^j$, and $\bar{y}_2^j$ are left out of the minimization scheme; it turns out that $\bar{z}_1^j$, $\bar{x}_2^j$, and $\bar{z}_2^j$ are three independent parameters fully specifying the molecule's orientation. We actually solve equations $(f_j=0)$ rather than merely fit in its usual sense (minimize f_j). Knowledge on the values $(\alpha_j,\beta_j,\gamma_j)$ finally allows one to draw the molecules in their actual orientations by applying the coordinate transformation $\vec{r}\,'=\mathfrak{R}_{zyz}(\alpha_j,\beta_j,\gamma_j)\vec{r}$. The resulting $5\times1\times1$ supercell is shown in Fig. 9(b).

The eight orientations $A_1,\ldots,B_4$ display a striking resemblance to the low-T orientations in C_{60} fullerite [see Figs. 9(b) and 10]. To quantify the deviations from orientations I–IV, we convert Euler angles to Euler parameters. The Euler parameters $(e_0,\vec{e}=(e_1,e_2,e_3))$ are defined as

$$e_0=\cos\frac{\phi}{2}, \tag{A4a}$$

$$\vec{e}=\vec{p}\,\sin\frac{\phi}{2} \tag{A4b}$$

for a rotation over ϕ about the normalized vector $\vec{p}$. Note that the relation $e_0^2+e_1^2+e_2^2+e_3^2=1$ holds. For the corresponding rotation matrix we write $\mathfrak{R}(e_0,\vec{e})$. Orientations I–IV have $\phi=22.0°$ and $\vec{p}_{\rm I}=1/\sqrt{3}(1,1,1)$, $\vec{p}_{\rm II}=1/\sqrt{3}(1,-1,-1)$, $\vec{p}_{\rm III}=1/\sqrt{3}(-1,-1,1)$, and $\vec{p}_{\rm IV}=1/\sqrt{3}(-1,1,-1)$, respectively. To get the Euler parameters for orientations $A_1,\ldots,B_4$, we first average the Euler angles $(\alpha_j,\beta_j,\gamma_j)$ of equal orientations (e.g., for A_1, the average Euler angles are obtained by averaging over $t=4$ and 8) and then solved $\mathfrak{R}(e_0,\vec{e})=\mathfrak{R}_{zyz}(\alpha,\beta,\gamma)$ numerically for ϕ and $\vec{p}$. The resulting values, together with the average Euler angles, are listed in Table II. We have tabulated unnormalized rotation vectors $\tilde{\vec{p}}$ since we started the numerical search for solutions from the vectors $\vec{p}_{\rm I},\ldots,\vec{p}_{\rm IV}$ involving the value $1/\sqrt{3}=0.577\,350$. Up to the third decimal, the absolute values of corresponding components of all $\tilde{\vec{p}}$ vectors are identical for all four members of the two families; the rotation angles are 21.9° and 22.8° for A- and B-type orientations, respectively.

[1] S. Pekker, É. Kováts, G. Oszlányi, G. Bényei, G. Klupp, G. Bortel, I. Jalsovszky, E. Jakab, F. Borondics, K. Kamarás, M. Bokor, G. Kriza, K. Tompa, and G. Faigel, Nature Mater. **4**, 764 (2005).

[2] G. Bortel, G. Faigel, É. Kováts, G. Oszlányi, and S. Pekker, Phys. Status Solidi B **243**, 2999 (2006).

[3] A. Iwasiewicz-Wabnig, B. Sundqvist, É. Kováts, I. Jalsovszky, and S. Pekker, Phys. Rev. B **75**, 024114 (2007).

[4] C. A. Kuntscher, S. Frank, K. Kamarás, G. Klupp, É. Kováts, S. Pekker, G. Bényei, and I. Jalsovszky, Phys. Status Solidi B **243**, 2981 (2006).

[5] B. Verberck, V. Heresanu, S. Rouzière, J. Cambedouzou, P. Launois, É. Kováts, S. Pekker, G. A. Vliegenthart, K. H. Michel, and G. Gompper,

Fullerenes, Nanotubes, Carbon Nanostruct. **16**, 293 (2008).
[6] W. Krätschmer, L. D. Lamb, K. Fostiropoulos, and D. R. Huffman, Nature (London) **347**, 354 (1990).
[7] For an overview, see L. Forró and L. Mihály, Rep. Prog. Phys. **64**, 649 (2001).
[8] P. E. Eaton and T. W. Cole, Jr., J. Am. Chem. Soc. **86**, 3157 (1964).
[9] H. W. Kroto, J. R. Heath, S. C. O'Brien, R. F. Curl, and R. E. Smalley, Nature (London) **318**, 162 (1985).
[10] The interstitial voids of a fcc unit cell are surrounded by six lattice points being the vertices of a regular octahedron.
[11] B. Verberck, J. Cambedouzou, P.-A. Albouy, S. Rouziére, V. Heresanu, É. Kováts, S. Pekker, and P. Launois (unpublished).
[12] R. Tycko, R. C. Haddon, G. Dabbagh, S. H. Glarum, D. C. Douglass, and A. M. Mujsce, J. Phys. Chem. **95**, 518 (1991).
[13] R. M. Fleming, T. Siegrist, P. M. Marsh, B. Hessen, A. R. Kortan, D. W. Murphy, R. C. Haddon, R. Tycko, G. Dabbagh, A. M. Mujsce, M. L. Kaplan, and S. M. Zahurak, Mater. Res. Soc. Symp. Proc. **206**, 691 (1991).
[14] C. S. Yannoni, R. D. Johnson, G. Meijer, D. S. Bethune, and J. R. Salem, J. Phys. Chem. **95**, 9 (1991).
[15] D. A. Neumann, J. R. D. Copley, R. L. Cappelletti, W. A. Kamitakahara, R. M. Lindstrom, K. M. Creegan, D. M. Cox, W. J. Romanov, N. Coustel, J. P. McCauley, Jr., N. C. Maliszewskyj, J. E. Fischer, and A. B. Smith III, Phys. Rev. Lett. **67**, 3808 (1991).
[16] P. Launois, S. Ravy, and R. Moret, Phys. Rev. B **52**, 5414 (1995).
[17] A. Dworkin, H. Szwarc, S. Leach, J. P. Hare, T. J. S. Dennis, H. W. Kroto, R. Taylor, and D. R. M. Walton, C. R. Acad. Sci. III **213**, 979 (1991).
[18] P. A. Heiney, J. E. Fischer, A. R. McGhie, W. J. Romanov, A. M. Denenstein, J. P. McCauley, Jr., A. B. Smith III, and D. E. Cox, Phys. Rev. Lett. **66**, 2911 (1991).
[19] R. Sachidanandam and A. B. Harris, Phys. Rev. Lett. **67**, 1467 (1991).
[20] P. A. Heiney, J. E. Fischer, J. P. McCauley, Jr., A. B. Smith III, and D. E. Cox, Phys. Rev. Lett. **67**, 1468 (1991).
[21] W. I. F. David, R. M. Ibberson, J. C. Matthewman, K. Prassides, T. J. S. Dennis, J. P. Hare, H. W. Kroto, R. Taylor, and D. R. M. Walton, Nature (London) **353**, 147 (1991).
[22] A. B. Harris and R. Sachidanandam, Phys. Rev. B **46**, 4944 (1992).
[23] The value reported in Ref. 21 is $\phi=-98°$ which is, taking into account threefold symmetry, equivalent to $-98°+120°=+22°$.
[24] P. W. Stephens, G. Bortel, G. Faigel, M. Tegze, A. Jánossy, S. Pekker, G. Oszlányi, and L. Forró, Nature (London) **370**, 636 (1994).
[25] P. Launois, R. Moret, J. Hone, and A. Zettl, Phys. Rev. Lett. **81**, 4420 (1998); P. Launois, R. Moret, E. Llusca, J. Hone, and A. Zettl, Synth. Met. **103**, 2354 (1999).
[26] A. Huq, P. W. Stephens, G. M. Bendele, and R. M. Ibberson, Chem. Phys. Lett. **347**, 13 (2001).
[27] S. Rouzière, S. Margadonna, K. Prassides, and A. N. Fitch, Europhys. Lett. **51**, 314 (2000).
[28] C. Coulon, A. Pénicaud, R. Clérac, R. Moret, P. Launois, and J. Hone, Phys. Rev. Lett. **86**, 4346 (2001).
[29] B. Verberck, A. V. Nikolaev, and K. H. Michel, Phys. Rev. B **71**, 165117 (2005).
[30] D. Frenkel and B. Smit, *Understanding Molecular Simulation—From Algorithms to Applications*, 2nd ed. (Academic, San Diego, 2002).
[31] K. Binder and D. Landau, *A Guide to Monte Carlo Simulations in Statistical Physics*, 2nd ed. (Cambridge University Press, Cambridge, 2005).
[32] If $U^n \leq U^o$ then accept, if $U^n > U^o$ then accept with probability $\exp -(U^n-U^o)/k_BT$. Here, U coincides with the total energy E for the canonical ensemble (NVT-ensemble) and equals $E+pV-Nk_BT \ln V$ for the isothermal-isobaric ensemble (NpT-ensemble), and the superscripts n and o stand for the old and the new configurations, respectively.
[33] These are average values since the control flow of the program decides whether to change a molecule (translation or orientation) or the volume on a random number basis (respecting the 10 000/10 ratio).
[34] A. Cheng and M. L. Klein, Phys. Rev. B **45**, 1889 (1992); M. Sprik, A. Cheng, and M. L. Klein, J. Phys. Chem. **96**, 2027 (1992); J. P. Lu, X.-P. Li, and R. M. Martin, Phys. Rev. Lett. **68**, 1551 (1992); X.-P. Li, J. P. Lu, and R. M. Martin, Phys. Rev. B **46**, 4301 (1992).
[35] D. Lamoen and K.H. Michel, Z. Phys. B: Condens. Matter **92**, 323 (1993).
[36] P. Launois, S. Ravy, and R. Moret, Phys. Rev. B **55**, 2651 (1997).
[37] D. Lamoen and K. H. Michel, J. Chem. Phys. **101**, 1435 (1994).
[38] T. Yildirim, P. M. Gehring, D. A. Neumann, P. E. Eaton, and T. Emrick, Phys. Rev. Lett. **78**, 4938 (1997).
[39] K. H. Michel, J. R. D. Copley, and D. A. Neumann, Phys. Rev. Lett. **68**, 2929 (1992).
[40] A. Cheng and M. L. Klein, J. Phys. Chem. **95**, 6750 (1991).
[41] L. A. Girifalco, J. Phys. Chem. **96**, 858 (1992).
[42] N. L. Allinger, J. Am. Chem. Soc. **99**, 8127 (1977).
[43] A. V. Nikolaev, B. Verberck, and G. V. Ionova, "Molecular interaction energies and optimal configuration of a cubane dimer," Int. J. Quantum Chem. (to be published).
[44] V. R. Coluci, F. Sato, S. F. Braga, M. S. Skaf, and D. S. Galvão, J. Chem. Phys. **129**, 064506 (2008).
[45] There is a subtlety concerning the low-T structure of C_{60} fullerite. As shown by Harris and Sachidanandam (Ref. 22), there are two realizations of its space group ($Pa\bar{3}$). The two variants are related to each other by an inversion followed by mirroring about the $(1\bar{1}0)$ plane (or, equivalently, a rotation over π about the $[1\bar{1}0]$ direction). If we identify the structure shown in Fig. 2 as the first variant, then the structure shown in Fig. 10(b) is the second variant.
[46] C. J. Bradley and A. P. Cracknell, *The Mathematical Theory of Symmetry in Solids* (Clarendon, Oxford, 1972).